Nanoscale

Accepted Manuscript

This article can be cited before page numbers have been issued, to do this please use: J. Liu, C. DETREMBLEUR, A. Debuigne, M. DE PAUW-GILLET, S. Mornet, L. Vander Elst, S. Laurent, C. Labrugère, E. Duguet and C. JEROME, *Nanoscale*, 2013, DOI: 10.1039/C3NR02861E.

This is an *Accepted Manuscript*, which has been through the RSC Publishing peer review process and has been accepted for publication.

Accepted Manuscripts are published online shortly after acceptance, which is prior to technical editing, formatting and proof reading. This free service from RSC Publishing allows authors to make their results available to the community, in citable form, before publication of the edited article. This *Accepted Manuscript* will be replaced by the edited and formatted *Advance Article* as soon as this is available.

To cite this manuscript please use its permanent Digital Object Identifier (DOI®), which is identical for all formats of publication.

More information about *Accepted Manuscripts* can be found in the **Information for Authors**.

Please note that technical editing may introduce minor changes to the text and/or graphics contained in the manuscript submitted by the author(s) which may alter content, and that the standard **Terms & Conditions** and the **ethical guidelines** that apply to the journal are still applicable. In no event shall the RSC be held responsible for any errors or omissions in these *Accepted Manuscript* manuscripts or any consequences arising from the use of any information contained in them.

Nanoscale

Dynamic Article Links ►
View Article Online
DOI: 10.1039/C3NR02861E

Cite this: DOI: 10.1039/c0xx00000x

www.rsc.org/xxxxxx

PAPER

Poly(acrylic acid)-*block*-poly(vinyl alcohol) Anchored Maghemite Nanoparticles Designed for Multi-stimuli Triggered Drug Release†

Ji Liu,[a,c] Christophe Detrembleur,*[a] Antoine Debuigne,[a] Marie-Claire De Pauw-Gillet,[b] Stéphane Mornet,[c] Luce Vander Elst,[d] Sophie Laurent,[d] Christine Labrugère,[c,e] Etienne Duguet*[c] and Christine Jérôme*[a]

Received (in XXX, XXX) Xth XXXXXXXXX 20XX, Accepted Xth XXXXXXXXX 20XX
DOI: 10.1039/b000000x

Original core/corona nanoparticles composed of a maghemite core and a stimuli-responsive polymer coating made of poly(acrylic acid)-*block*-poly(vinyl alcohol) macromolecules were fabricated for drug delivery system (DDS) application. This kind of DDS aims to combine the advantage of stimuli-responsive polymer coating, in order to regulate the drug release behaviours under different conditions, furthermore, improve the biocompatibility and *in vivo* circulation half-time of the maghemite nanoparticles. Drug loading capacity was evaluated with methylene blue (MB), a cationic model drug. Triggered release of MB was studied under various stimuli such as pH, ionic strength or temperature. Local heating generated under alternative magnetic field (AMF) application was studied, and remotely AMF-triggered release was also confirmed, while a mild heating-up of the release medium was observed. Furthermore, their potential application as magnetic resonance imaging (MRI) contrast agents was explored via relaxivity measurements and T_2-weighted images acquisition. Preliminary studies on the cytotoxicity against mouse fibroblast-like L929 cell line and also their cellular uptake within human melanoma MEL-5 cell line were carried out. In conclusion, this kind of stimuli-responsive nanoparticles appears to be promising carriers for delivering drugs to some tumour sites or into cellular compartments with acidic environment.

Introduction

Chemotherapy is currently indispensable in most cancer treatments. However, due to the huge side-effects of current clinical anticancer drugs, it is of great significance to protect the body tissues and organs from the potential toxicity before the drugs reach the specifically-desirable sites. In the past decades, much effort has been devoted to load those chemotherapeutic agents within different kinds of vehicles in order to achieve an idealistic drug delivery system (DDS).[1] Various structures have been investigated for this application such as polymeric micelles, liposomes, hydrogels, and inorganic/organic core/corona nanoparticles.[1,2] The latter, made of an inorganic core and a stimuli-responsive polymer corona, have been frequently suggested as promising vehicles to deliver drugs or genes thanks to their outstanding biocompatibility, physico-chemical stability, versatile surface modifications, capability to release the cargos responding to external stimuli, *etc*.[3,4]

Some magnetic nanoparticles, *e.g.* maghemite (γ-Fe_2O_3) and magnetite (Fe_3O_4), have found various current or future applications in the biomedical field, such as MRI contrast agents, hyperthermia mediators under alternating magnetic field (AMF), biosensors, DDS components, *etc.*, due to the original combination of magnetic properties and biocompatibility.[5-7] For instance, they can be guided within biological tissues under external magnetic field gradients, providing a potential platform for magnetically-guided delivery.[8,9] Moreover, their capability to generate a local heating under AMF, via mechanisms such as Néel relaxation, Brownian relaxation or hysteresis losses, opens new routes to trigger the drug release.[10-13] However, these nanoparticles suffer from a lack of colloidal stability in biological fluids and they might be rapidly cleared from the bloodstream before reaching their targets.[14] In order to overcome these obstacles, coating with appropriate functional macromolecules has been widely attempted, especially if the combination also allows to integrate several functions,[15] such as magnetism with fluorescence,[16] pH-responsiveness,[17] thermo-responsiveness,[18] *etc*.

Poly(acrylic acid) (PAA) is a well-known polyelectrolyte, which is capable of undergoing reversible conformational transitions responding to external variations of pH or ionic strength (IS).[19-21] Generally, for pH values above the pK_a of PAA (4.5), the pendant carboxylic acid groups are de-protonated and hydrated leading to a randomly coiled conformation due to the electrostatic repulsion between the carboxylate moieties. In contrast, for pH values below pK_a, the groups are protonated leading to a PAA polymer chain with a dehydrated globular conformation. Moreover, these polymer chains might adopt a randomly coiled conformation at high IS whereas globular conformation at low IS above the pK_a.[22-25] Some PAA-based

View Article Online
DOI: 10.1039/C3NR02861E

macromolecules have already been utilized to stabilize nanoparticles for DDS applications, such as gold nanorods,[26] magnetite,[27,28] maghemite,[21,29] gold nanospheres,[30-32] silica,[33, 34] *etc*. It is widely reported that those nano-scaled DDS could be easily taken up by the cells via the endocytosis process,[35,36] which starts at physiological pH of 7.4, drops to lower pH of 5.5 ~ 6.0 in endosomes and finally approaches 5.0 in lysosomes.[37] Therefore, if this kind of pH-responsive nanoparticles was used as DDS, the change in pH during the endocytosis process could also be envisaged as a stimulus to trigger the drug release with an improved efficiency. However, due to their dehydrated essence under pH values below the pK_a, nanoparticles coated with pH-responsive homopolymers became unstable and flocculation was observed.[26,27,31,38,39]

In this work, a poly(acrylic acid)-*b*-poly(vinyl alcohol) (PAA-*b*-PVOH) double-hydrophilic block copolymer, with a pH- and IS-responsive block (PAA) and non-ionic block (PVOH), was used for the first time to stabilize 7.5-nm maghemite nanoparticles (γ-Fe_2O_3 NPs). The colloidal stability of the resultant γ-Fe_2O_3@PAA-*b*-PVOH NPs was expected to be improved at pH values below the pK_a of PAA, due to the presence of the PVOH block that is not pH-sensitive and known to ensure steric stabilization in aqueous medium. The pH- and ionic strength-responsiveness of the γ-Fe_2O_3@PAA-*b*-PVOH NPs was studied by dynamic light scattering (DLS). The capacity to upload a cationic model drug (methylene blue, MB) and to trigger its release under different conditions was then investigated. Due to their superparamagnetic properties, the potential application of the γ-Fe_2O_3@PAA-*b*-PVOH NPs for remotely magnetically-triggered drug release and as MRI contrast agents were also explored. Cytotoxicity assessment of the γ-Fe_2O_3@PAA-*b*-PVOH NPs against mouse fibroblast-like L929 cells was evaluated via the MTS assay, and preliminary studies on cellular uptake within human melanoma MEL-5 cells were also carried out.

Materials and methods

Materials

Iron (II) chloride tetrahydrate ($FeCl_2{\cdot}4H_2O$, 99%), iron (III) chloride hexahydrate ($FeCl_3{\cdot}6H_2O$, 97%), ammonium hydroxide solution ($NH_3{\cdot}H_2O$, 28.0 *wt*.%), sodium hydroxide (NaOH, 90%), hydrogen chloride (HCl, 37%), nitric acid (HNO_3, 70%), *N*-hydroxysuccinimide (NHS, 98%), sodium acetate trihydrate ($NaAc{\cdot}3H_2O$, 99.0%), 4',6'-diamidino-2-phenylindole (DAPI, 98.0%), fluoresceinamine (FA, 75%), sodium chloride (NaCl, 98%) and 1-ethyl-3-(3-dimethylaminopropyl)carbodiimide hydrochloride (EDC, 97%) were purchased from *Aldrich*. GIBCO Dulbecco's modified Eagle medium (DMEM, low glucose), L-glutamine, PBS buffer solution (without Ca^{2+} and Mg^{2+}), foetal bovine serum (FBS) and trypsin were obtained from BioWhittaker (Walkersville, MD). 3-(4,5-dimethylthiazol-2-yl)-5-(3-carboxymethoxyphenyl)-2-(4-sulfophenyl)-2H-tetrazolium (MTS) was obtained from *Promega* (Madison, USA). PBS buffer solution (with Ca^{2+} and Mg^{2+}), penicillin and streptomycin were purchased from GIBCO BRL (Gaithersburg, MD).

Methods

Preparation of PAA-b-PVOH copolymers: they were obtained via the complete hydrolysis of the poly(acrylonitrile)-*b*-poly(vinyl acetate) macromolecules (PAN-*b*-PVAc), which were synthesized with PVAc-Co(acac)$_2$ as macro-initiators to polymerize acrylonitrile. Full description of the polymer synthesis and analyses were previously reported.[20] Herein, PAA_{59}-*b*-$PVOH_{197}$ (PDI 1.07) was used (PAA-*b*-PVOH in the following context refers to the PAA_{59}-*b*-$PVOH_{197}$ copolymer). Fluoresceinamine-labelled PAA-*b*-PVOH copolymers were prepared via the amidation reaction between the AA groups and fluoresceinamine molecules. Typically, PAA-*b*-PVOH (100 mg, 0.56 mmol AA monomer units) and fluoresceinamine (16.8 μmol) (FA/AA = 3/100 *mol./mol.*) were added into 20 mL of deionized water, with NHS (16.8 μmol)/EDC (16.8 μmol) as catalysts in dark. After 24 h, the product was purified via 48-h dialysis against de-ionized water, and the resultant FA-labelled PAA-*b*-PVOH copolymer was freeze-dried and light yellow powders were recovered. A grafting degree of *ca*. 1.4 *mol.*% (AA-FA monomer units out of overall AA monomer units) was estimated from ^{1}H NMR analysis (See ESI, Fig. S1†).

Preparation of the γ-Fe_2O_3 NPs: according to the Massart's method,[40] 3.5 L of iron (III) precursor ($FeCl_3{\cdot}6H_2O$, 0.32 mol) and iron (II) precursor ($FeCl_2{\cdot}4H_2O$, 0.16 mol) in de-ionized water were mixed with 300 mL of ammonium hydroxide solution (NH_4OH, 8.6 M) at room temperature, resulting in the mixture turning black immediately. After 15 min, the nanoparticles were collected with a permanent neodymium magnet, and the supernatant was discarded. The nanoparticles were then suspended in 400 mL of nitric acid solution (2 M) under stirring for another 15 min. After collection of the nanoparticles and removal of the supernatant, 600 mL of ferric nitrate solution (0.33 M) were added and stirred at 90°C for 30 min. Then, they were peptized with 400 mL of nitric acid (2 M) for 15 min at room temperature, and after rinsing with acetone (200 mL) for 5 times, the particles were dispersed in 500 mL of de-ionized water. pH value of the final γ-Fe_2O_3 NPs suspension was tuned to be *ca*. 4.0, and a concentration of 61.5 g/L was confirmed by titration.

Preparation of γ-Fe_2O_3@PAA-b-PVOH NPs: 30 mg of the γ-Fe_2O_3 NPs were re-dispersed in 10 mL of PBS buffer (pH 6.5, 10 mM) under sonication (20 min), while 30 mg of the PAA-*b*-PVOH copolymer were dissolved in PBS buffer (10 mM, pH 6.5). Both solutions were then mixed under stirring for 12 h at room temperature. The excess of copolymer was removed by three centrifugation/rinsing cycles (12,000 rpm, 20 min), and the γ-Fe_2O_3@PAA-*b*-PVOH NPs were then re-suspended in de-ionized water. Freeze-dried nanoparticles were used to determine the polymer fraction via thermogravimetric analysis (TGA, *ca*. 12 *wt*.%, See ESI, Fig. S2†). The FA-labelled γ-Fe_2O_3@PAA-*b*-PVOH NPs were also prepared via the above-mentioned protocol, but carried out in the dark.

Uploading and triggered release of methylene blue in different buffer solutions: methylene blue (MB) was uploaded to the PAA-*b*-PVOH coating via electrostatic interaction with the carboxylate groups of the PAA blocks. Typically, 30 mg of γ-Fe_2O_3@PAA-*b*-PVOH NPs in 25 mL of PBS buffer (pH 7.4, 10 mM) and 5 mL of MB/PBS solution (5×10^{-5} M, pH 7.4) were mixed and stirred overnight at room temperature. After removing the free MB molecules by three centrifugation-rinsing (12,000 rpm, 15 min) cycles, the MB-loaded γ-Fe_2O_3@PAA-*b*-PVOH NPs were re-dispersed in PBS buffer (pH 7.4, 10 mM).

View Article Online
DOI: 10.1039/C3NR02861E

Uploading amount of MB was quantified by measuring the absorbance of the depleted supernatant at 665 nm with a UV/*vis* spectrometer, thanks to the pre-determined calibration curve (See ESI, Fig. S3†). Drug loading capacity (*DLC*) and drug loading efficiency (*DLE*) were calculated to evaluate the uploading capability of the guest molecules:

$$DLC(\%) = \frac{mass\ of\ loaded\ MB}{mass\ of\ \gamma - Fe_2O_3@PAA - b - PVOH\ NPs} * 100$$

$$DLE(\%) = \frac{mass\ of\ loaded\ MB}{mass\ of\ fed\ MB} * 100$$

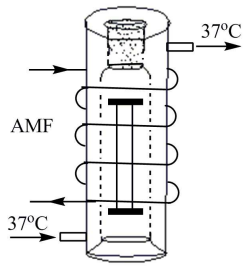

Fig. 1 Apparatus designed for the AMF-triggered release: internal diameter 2 cm, external diameter 4 cm, internal height 11 cm, external height 14 cm, volume of inner reservoir: *ca*. 35 cm^3. Nanoparticles suspension in dialysis bag was placed in the center of the magnetic field coils, a 37ºC water bath was circulating during the experiments, and a thermo-sensor was introduced from the upper opening to detect the temperature of release medium.

To follow the release profiles, 5 mL of the MB-loaded γ-Fe_2O_3@PAA-*b*-PVOH suspension were put in dialysis bag (cut-off of 3,500 Da) against 20 mL of buffer solutions with different pH values, ionic strengths or temperatures with/without AMF (755 kHz, 14 mT) application in an apparatus as shown in Fig. 1. At each pre-determined interval, 0.5 mL of the release medium was sampled, while 0.5 mL of fresh buffer solution was added to keep a fixed volume. Three different buffers, PBS buffer (pH 7.4, 10 mM), NaAc/HCl buffer (pH 5.0, 10 mM) and NaAc/HCl buffer (pH 4.5, 10 mM) were used, and buffer solutions with different ionic strengths were obtained by changing the concentration of NaCl. The amount of released MB was also quantified spectrophotometrically with the MB calibration curve (See ESI, Fig. S3†). The release profiles were presented in a cumulative mode, and the error bar in each profile represented standard deviation from three independent experiments.

Cell culture and cytotoxicity assessment: the mouse fibroblast-like L929 cell line was obtained from ATCC (ATCC CCL-1), and the cells were cultured at 37°C under humidified air (5% CO_2) in Dulbecco's modified Eagle medium (DMEM), which was supplemented with 5 *vol.*% of heat-inactivated FBS, 1 *vol.*% of glutamax, 1 *vol.*% of penicillin/streptomycin (10,000 units of penicillin and 10,000 units of streptomycin/mL before use) (DMEM complete medium). The human melanoma MEL-5 cells (originated from a non pigmented clone 32, gift from Dr. G. Degiovanni, University of Liège) were also cultured in DMEM complete medium. After rinsing with PBS (Ca^{2+}/Mg^{2+} free) buffer solution, the cells were detached with trypsin (0.2 *vol.*%)/PBS (Ca^{2+}/Mg^{2+} free) buffer solution.

For the cytotoxicity assessment, the L929 cells were seeded in a 96-well plate at a density of 5×10^3 cells/well, and grown in DMEM complete medium for another 24 h. Then after removal of the medium, the cells were treated with the γ-Fe_2O_3@PAA-*b*-PVOH NPs suspension in DMEM medium with different concentrations (1000, 100, 10 and 1 μg/mL) for periods of 24 h or 48 h. For each incubation concentration, 5 parallel samples were carried out at the same time. After each pre-determined incubation period, the cells were rinsed with PBS (with Ca^{2+}/Mg^{2+}) buffer solution, and cell viability was evaluated via the MTS assay. 20 μL of MTS and 100 μL of PBS (with Ca^{2+}/Mg^{2+}) buffer solution were added for each well, and then the plates were incubated for 30 min at 37°C. The absorbance at 490 nm was measured using a Power wave X (Biotek instrument Inc.) micro-plate reader. Percentage cell viabilities were determined relative to the untreated cells (control, 100% viability), and the bar graphs of cytotoxicity profiles were presented as mean values ± standard deviation from five independent samples.

Qualitative studies on cellular uptake with confocal laser scanning microscopy (CLSM): MEL-5 cells (3.8×10^5) were seeded in a 12-well plate with 2 mL of DMEM complete medium. After 24 h, the medium was replaced with 2 mL of FA-labelled γ-Fe_2O_3@PAA-*b*-PVOH NPs suspension (20, 50, 100 or 200 μg/mL) in DMEM complete medium. After incubating for a pre-determined period (3, 6, 15 or 24 h), the suspension was removed and the cells were rinsed twice with PBS (with Ca^{2+}/Mg^{2+}) buffer solution to eliminate those free nanoparticles. Then the cells were treated with paraformaldehyde (4 *vol.*%)/DAPI (1 *vol.*%)/PBS (Ca^{2+}/Mg^{2+} free) buffer solution at room temperature for 15 min in dark. After rinsing with PBS (with Ca^{2+}/Mg^{2+}) buffer solution for another two times, 2 mL of PBS (with Ca^{2+}/Mg^{2+}) buffer solution were added. Analyses of the treated MEL-5 cells were conducted with a CLSM (Nikon, A1R hybrid resonant), equipped with an argon laser using a FITC filter (*Ex*: 488 nm and *Em*: 525 nm).

Qualitative studies on cellular uptake with transmission electron microscopy (TEM): MEL-5 cells internalized with γ-Fe_2O_3@PAA-*b*-PVOH NPs were obtained according to the above-mentioned protocol. After detachment with trypsin (0.2 *vol.*%)/PBS (Ca^{2+}/Mg^{2+} free) buffer solution, centrifugation (1,300 rpm, 5 min), and rinsing with fresh PBS (Ca^{2+}/Mg^{2+} free) buffer solution, the treated cells were fixed with glutaraldehyde (4 *wt.*%)/PBS buffer solution (Ca^{2+}/Mg^{2+} free) at room temperature. Then the cell pellet was rinsed with PBS (Ca^{2+}/Mg^{2+} free) buffer solution again to remove the free fixatives, dehydrated in alcohol series, embedded in Epon, and then sliced (*ca*. 70 nm in thickness) for TEM observation.

Quantitative studies on the cellular uptake with cytofluorometer: MEL-5 cells internalized with the γ-Fe_2O_3@PAA-*b*-PVOH NPs were also obtained according to the above-mentioned protocol. After detachment with trypsin (0.2 *vol.*%)/PBS (Ca^{2+}/Mg^{2+} free) buffer solution and centrifugation (1,300 rpm, 5 min), the treated cells were re-dispersed in fresh PBS (Ca^{2+}/Mg^{2+} free) buffer solution. The treated cells were analyzed with a FACScan fluorescence-activated cell sorter (FACS, Becton-Dickinson). Fluorescence intensities and the percentage of cell-associated fluorescence were determined by using the CellQuest software. 400 μL of treated MEL-5 cells in PBS (with Ca^{2+}/Mg^{2+}) buffer solution was used for this analysis, while untreated MEL-5 cells were taken as a blank. The ratio of

View Article Online
DOI: 10.1039/C3NR02861E

fluorescence intensity of 10,000 treated MEL-5 cells to that of 10,000 untreated cells was expressed as mean fluorescence intensity (MFI). The bar graphs in the MFI patterns represented mean values ± standard deviation from three independent experiments.

Statistical analysis: cell culture experiments were performed in triplicate. Results were presented as mean values ± standard deviation. Statistical analyses of the data were performed using the unpaired and two tailed Student's *t*-test. Statistical significance was determined at $p < 0.05$.

Characterization

Dynamic light scattering (DLS) measurements were carried out with a Malvern Instrument Nano-ZS, which was equipped with a He-Ne laser (λ = 663 nm) and scattering angle of 90° at 25°C. The correlation function was analysed with the CONTIN method, and hydrodynamic diameter (D_h) was determined using the Stokes-Einstein equation. Standard deviation was used to evaluate the size distribution (PDI). Electrophoretic mobility of the γ-Fe_2O_3@PAA-*b*-PVOH NPs was checked at 25°C and zeta potential (ζ) was obtained with the Smoluchowski approximation. The average D_h and ζ was obtained by averaging data from three different runs.

UV/vis spectra of the γ-Fe_2O_3@PAA-*b*-PVOH NPs, FA-labelled γ-Fe_2O_3@PAA-*b*-PVOH NPs and MB-loaded γ-Fe_2O_3@PAA-*b*-PVOH NPs aqueous suspension (50 μg/mL), and also MB aqueous solution (3 μM) were recorded between 200 and 900 nm with a Hitachi U-3300 spectrophotometer.

Transmission electron microscopy (TEM) was performed with a Philips CM-100 microscope. A drop of the nanoparticles aqueous suspension was placed onto a copper grid and left to dry under air. The average size and size distribution were obtained by statistically sampling *ca*. 200 particles.

Fourier transform infrared spectra (FTIR) of the γ-Fe_2O_3@PAA-*b*-PVOH NPs, bare γ-Fe_2O_3 NPs and PAA-*b*-PVOH copolymer were performed with a Perkin Elmer FTIR instrument. Samples were mixed and grinded with potassium bromide, and then compressed for FTIR analysis.

Magnetization measurements of the γ-Fe_2O_3@PAA-*b*-PVOH and bare γ-Fe_2O_3 NPs were conducted with a 5MPMS superconducting quantum interference device (SQUID) in the field range of -6,000 to 6,000 Oe at 300 K.

AMF-induced heating experiments were performed at 755 kHz, and 14 mT in a magnetic field coil (35 mm × 4 turns). An Eppendorf tube containing 1.5 mL of the nanoparticles aqueous suspension with a known concentration was placed in the centre of the coil, and the heating process was monitored with a fibre optical thermo-sensor to trace the change in temperature.

Proton relaxometry measurements of the γ-Fe_2O_3@PAA-*b*-PVOH NPs were performed with a Stelar Fast Field-Cycling Spectrometer FFC-2000 equipped with a permanent magnet for the relaxation measurements in the range of 0.01 ~ 40 MHz at 37°C. Additional data (T_1 and T_2) were obtained at 20 and 60 MHz on Bruker Minispec mq20 and mq60, respectively.

Results and discussion

Preparation of the γ-Fe_2O_3@PAA-*b*-PVOH NPs

Maghemite (γ-Fe_2O_3) nanoparticles were prepared from the well-established Massart's method.[40] Briefly, the Fe(II) and Fe(III) precursors were co-precipitated into magnetite (Fe_3O_4) nanoparticles, and then further oxidized into maghemite nanoparticles. The morphology and size of the as-prepared γ-Fe_2O_3 NPs were characterized by TEM (See ESI, Fig. S4a†). An averaged diameter of *ca*. 7.5 nm was observed, in agreement with the previous report,[40] while an average hydrodynamic diameter (D_h) of *ca*. 30 nm (PDI 0.07) was also confirmed by DLS (See ESI, Fig. S4b†). XRD pattern (See ESI, Fig. S5a†) of the γ-Fe_2O_3 NPs is close to that of previous report of maghemite,[41] and isoelectric point (IEP) was confirmed to be *ca*. 7.0 (See ESI, Fig. S5b†). Immobilization of PAA-*b*-PVOH copolymer onto the γ-Fe_2O_3 NPs surface was carried out in PBS buffer solution (pH 6.5) via electrostatic interactions between the de-protonated PAA block and the positively-charged γ-Fe_2O_3 NPs (Scheme 1). Similarly to SiO_2@[poly(ethylene glycol)-*b*-poly(L-lysine)] NPs,[42] it was conjectured that the PAA-*b*-PVOH polymer chains might also form a typical anchor (PAA)-buoy (PVOH) conformation on the surface of γ-Fe_2O_3 NPs. Hence, a further-improved colloidal stability was achieved through electrostatic repulsion originating from the de-protonated PAA block and steric repulsion from PVOH block. A ζ value of -35 mV was detected for the γ-Fe_2O_3@PAA-*b*-PVOH NPs at pH 7.0, while 0 for the pure γ-Fe_2O_3 NPs (See ESI, Fig. S5b†).

The so-formed γ-Fe_2O_3@PAA-*b*-PVOH NPs were first characterized by transmission electron microscopy (TEM) (Fig. 2a), and nearly the same average diameter (*ca*. 7.5 nm) was observed as that of the bare γ-Fe_2O_3 NPs. The polymer shell was not visible by TEM, due to the lack of electron density and limited shell thickness after drying. However, D_h as determined by DLS increased sharply from 30 nm (PDI 0.07, pH 7.0) to 120 nm (PDI 0.11, pH 7.0) at after polymer coating (See ESI, Fig. S4b†). A polymer content of *ca*. 12 *wt*.% was confirmed by TGA analysis of the purified NPs (See ESI, Fig. S2†). The main IR characteristic bands, originating from both γ-Fe_2O_3 NPs and PAA-*b*-PVOH copolymer, are distinguishable in the FTIR spectra of the γ-Fe_2O_3@PAA-*b*-PVOH NPs (Fig. 2b). Moreover, a slight red-shift for carboxylic group from 1632 to 1650 cm^{-1} after coating might result from the electrostatic interactions between PAA blocks and γ-Fe_2O_3 NPs. The presence of the polymer coating was also confirmed by the fitted C1s peaks[43] and Fe2p peaks[44] from XPS analysis (See ESI, Fig. S6†).

Nanoscale

Dynamic Article Links ▶
View Article Online
DOI: 10.1039/C3NR02861E

Cite this: DOI: 10.1039/c0xx00000x

www.rsc.org/xxxxxx

PAPER

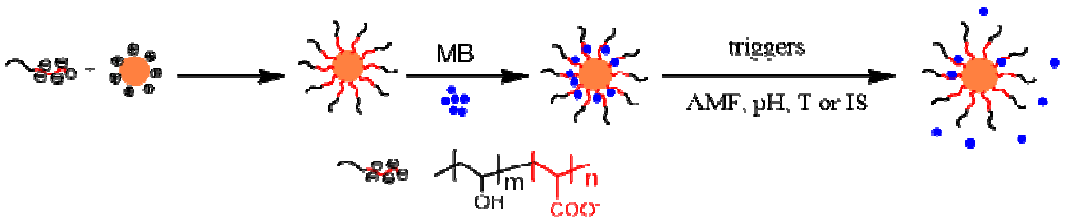

Scheme 1. Preparation of the γ-Fe_2O_3@PAA-*b*-PVOH NPs, loading of methylene blue (MB), and triggered release of MB in buffer solutions under variation in pH, ionic strength (IS), temperature or under alternative magnetic field (AMF) application.

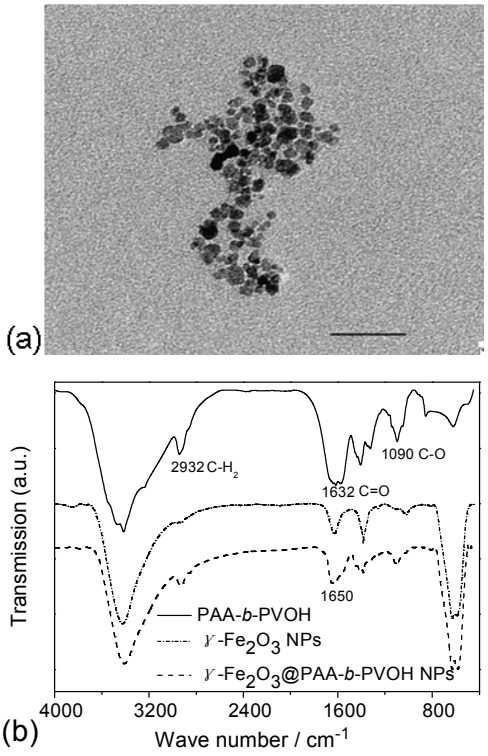

Fig. 2 (a) Representative TEM picture of the γ-Fe_2O_3@PAA-*b*-PVOH NPs (scale bar: 50 nm), and (b) FTIR spectra of the γ-Fe_2O_3@PAA-*b*-PVOH, bare γ-Fe_2O_3 NPs and PAA-*b*-PVOH copolymer.

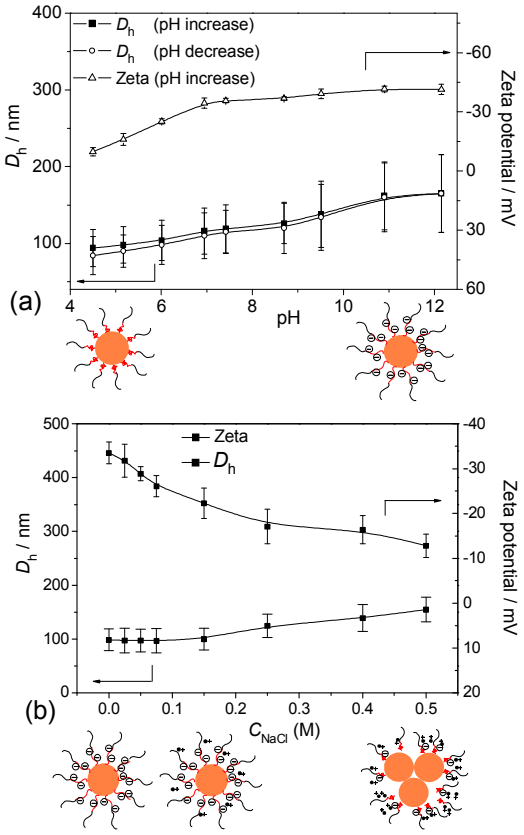

Fig. 3 Evolution of the hydrodynamic diameter (D_h) and zeta potential (ζ) *vs*. pH (a) and ionic strength (pH of 7.4, b) for the γ-Fe_2O_3@PAA-*b*-PVOH NPs (the solid lines just serve to guide the eyes. The error bars for hydrodynamic diameter represented standard deviation from independent 100 acquisitions, and error bars for zeta potential represented standard deviation from three independent measurements).

Stimuli-responsiveness of the γ-Fe_2O_3@PAA-*b*-PVOH NPs

The conformation of carboxylic-based polymers, *e.g.* PAA, is known to be very sensitive to pH variations.[20,45] Consequently, pH modulation is expected to affect the size and permeability of the polymer coating. As presented in other previous reports dealing with the pH-responsiveness of nanoparticles with homopolymer coatings, such as Au@poly(methacrylic acid),[26] Fe_3O_4@PAA,[27] γ-Fe_2O_3@PAA,[21,29] SWNT@PAA,[38] *etc.*, unstable dispersion and flocculation were observed in aqueous medium with pH values near the pK_a of PAA.

In our system, the PAA-*b*-PVOH copolymer was expected to improve the stability of the γ-Fe_2O_3@PAA-*b*-PVOH NPs, especially at lower pH values, *e.g.* pH near or below pK_a of PAA. To verify this hypothesis, DLS experiments were performed to study the pH-dependence of D_h and ζ of the γ-Fe_2O_3@PAA-*b*-PVOH NPs (Fig. 3a). pH was first set at 4.5, where the PAA

View Article Online
DOI: 10.1039/C3NR02861E

blocks were protonated avoiding any electrostatic repulsion between those nanoparticles. However, small D_h (80 nm) without flocculation was detected, even with a ζ of *ca*. 10 mV, similar to the stability reported with Fe_3O_4@PAMAM-*b*-PDMAEMA-*b*-PPEGMA[46] and Fe_3O_4@chitosan-*g*-(PEO-*b*-PPO-*b*-PEO) NPs.[47] Then upon increase in pH to 12 by gradually feeding a NaOH solution (0.1 M), both D_h and $|\zeta|$ increased due to the neutralization of carboxylic acid groups, and reached a plateau at pH value of *ca*. 10, due to the complete de-protonation of the PAA block, as shown in the scheme in Fig. 3a. High D_h of 180 nm and ζ of -40 mV were observed at pH value of 12, where PAA chains are fully deprotonated and therefore extended by electrostatic repulsion. These results showed that γ-Fe_2O_3@PAA-*b*-PVOH NPs are stable over a broad pH range, even at low pH as a result of the presence of pH-insensitive PVOH blocks.

To test the reversible pH-responsiveness, pH of the nanoparticles suspension was decreased again from pH 12 by gradually adding an HCl solution (0.1 N) (Fig. 3a). As expected, a decrease in D_h is observed, suggesting a reversible change in conformation leading to the collapse of the protonated PAA blocks. Moreover, compared to the first pH-increasing run, D_h was slightly lower in the second pH-decreasing run, which could be attributed to the effect of ionic strength (IS), which will be discussed in details later in Fig. 3b. It is worth noting that, by comparing D_h at pH of 5.0 (*ca*. 90 nm) and 7.4 (*ca*. 120 nm) in the first pH-increasing run without considering the effect of IS, D_h increased by *ca*. 1.33 times; hence, hydrodynamic volume (V_h) decreased by *ca*. 2.37 times after pH decreasing from 7.4 to 5.0, suggesting that an obvious de-swelling of the polymer corona might occur when pH decreases from 7.4 (human blood plasma value) to 5.0 (tumour sites, endosomes or lysosomes).[27,38] So it may be envisaged that this specific responsiveness to external pH variation might be used for triggered release of the pre-loaded guest molecules.

The conformation of the polyelectrolyte is also dependent on IS. It is known that excessive free ions may screen the intramolecular electrostatic repulsion, resulting in the coiling-up of the polymer chains.[19] Thus a decrease in D_h and a destabilization of the colloids might occur. The effect of colloidal properties of the γ-Fe_2O_3@PAA-*b*-PVOH NPs on IS was also studied by plotting D_h and ζ as a function of NaCl concentration (0.005 to 0.5 M) at pH 7.4 (Fig. 3b). At low IS values (< 0.08 M), a slight decrease in both D_h and ζ was observed, due to the electrostatic repulsive forces overreaching the attractive interactions. However, at higher IS values (> 0.25 M), due to the obvious shielding effect of external ions,[24,25] the attractive force might exceed the repulsive interaction, leading to the agglomeration between individual nanoparticles, as shown in the scheme in Fig. 3b, thus decrease in ζ and increase in D_h were detected. Importantly, the aggregates remained small and stable as the result of the stabilizing PVOH block presence.

Magnetic properties of γ-Fe_2O_3@PAA-*b*-PVOH NPs

Magnetization measurements of the nanoparticles before and after polymer coating were carried out at room temperature (See ESI, Fig. S7†). Saturation magnetization at 6000 Oe dropped from 57.0 to 50.6 emu/g after polymer coating. This may result from the decreased weight fraction of γ-Fe_2O_3 and non-magnetic character of the polymer coating, consistently with the γ-Fe_2O_3 fraction of 88 *wt*.% estimated by TGA (See ESI, Fig. S2†). Moreover, similar to the bare γ-Fe_2O_3 NPs, no hysteresis loop was detected at zero field for the γ-Fe_2O_3@PAA-*b*-PVOH NPs at 300 K (See ESI, Fig. S7† inset), corresponding to a superparamagnetic behaviour. Hence, this type of magnetic nanoparticles was supposed to be useful as heat mediators in AMF, thanks to Néel and/or Brownian relaxation mechanisms. Moreover, tumour cells could be killed at a temperature above 43°C via magnetic fluid hyperthermia (MFH), while the normal cells might be able to survive for a somewhat longer period.[7-9] Nevertheless, concentration of the nanoparticles has to be high enough to accomplish an efficient and homogeneous (at the tissue scale) temperature increase. That is why, for the moment, clinical developments of MFH remain rare. However, this heating capability could be also, and probably more easily, exploited to increase the local temperature of the drug reservoirs, hence, trigger the release of drug payloads. Thus, we evaluated the magnetic heating capability of the γ-Fe_2O_3@PAA-*b*-PVOH NPs by exposing their aqueous suspension to AMF (755 kHz, 14 mT) treatment. The evolution of temperature was followed as a function of AMF treatment period (Fig. 4). As shown, the temperature increased at a rate which is directly dependent on the concentration of magnetic nanoparticles. Specific loss power (SLP) was calculated according to the following formula:

$$SLP = \frac{c_p}{m_{Fe_2O_3}} * \frac{dT}{dt} \quad (1)$$

where c_p is the specific heat capacity of the suspension (assimilated to that of water: 4.186 J/(g·K)), d*T*/d*t* is the initial slope of the temperature *vs*. time when AMF was applied, *m* is the mass of the γ-Fe_2O_3@PAA-*b*-PVOH NPs. So, SLP value was estimated to be 23 W/(g of NPs). By taking into account their γ-Fe_2O_3 content (*ca*. 88 *wt*.%), a SLP of 26.1 W/(g of γ-Fe_2O_3) was calculated, close to 27.5 W/(g of γ-Fe_2O_3) for bare γ-Fe_2O_3 (curve not shown here). Because the SLP value is proportional to the square of the field strength (*H*) and also field frequency (*v*), usually it needs to be normalized to 1 MHz and 100 Oe for comparison with data from literature.[48] Here, the normalized value is *ca*. 25 W/(g Fe), comparable to previously reported data for the magnetic NPs with different sizes, such as 12 ~ 56 W/(g of Fe) (7.5 ~ 416 nm)[49] and 0.5 ~ 104 W/(g of Fe) (6 ~ 8 nm)[50].

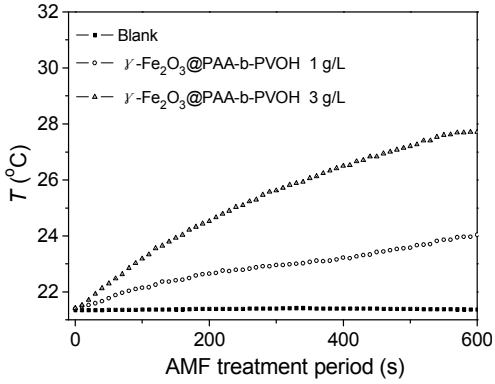

Fig. 4 Heating curves of the γ-Fe_2O_3@PAA-*b*-PVOH NPs suspensions with different concentrations under AMF treatment, while double-distilled de-ionized water was taken as a blank (18 mΩ).

View Article Online
DOI: 10.1039/C3NR02861E

Nuclear magnetic resonance dispersion (NMRD) relaxometry is well established for the relaxivity analysis of magnetic nanoparticle. Its advantage over the fixed-field measurements is that it could provide further insights into the dynamics of the magnetic moments and also the magnetic order of the nanoparticles. Fig. 5a shows the typical NMRD longitudinal relaxivity pattern (r_1 *vs.* v) of the γ-Fe_2O_3@PAA-*b*-PVOH NPs at pH of 7.4 at 37°C. Similar to bare γ-Fe_2O_3 NPs, the NMRD profile of the γ-Fe_2O_3@PAA-*b*-PVOH NPs was also levelled-off at low frequencies, then reached a maximum, and finally decreased rapidly at higher frequencies. The peak arose at $r_1(v)$ of *ca*. 3 MHz for γ-Fe_2O_3@PAA-*b*-PVOH NPs, while *ca*. 4 MHz for pure γ-Fe_2O_3 NPs. The shift of the peak towards lower frequencies might be attributed to the apparent increase of the radius due to the presence of polymer coating. In the same way the slight decrease in the maximum relaxivity can be related to the decreased magnetization due to the presence of polymer coating. To better understand the relaxivity behaviour, the NMRD profiles were fitted via the SPM theory developed by Muller and co-workers.[51] The simulated curves fit relatively well with the experimental NMRD profiles. From the fitting parameters (listed in the legend of Fig. 5), it can be seen that the parameters of saturated magnetization (M_s), crystal radius (D_{NMR}) and Néel relaxivity time ($\tau_{Néel}$) highlight the superparamagnetic essence of the γ-Fe_2O_3@PAA-*b*-PVOH NPs. Only a slight variation was detected before and after coating, indicating that the presence of PAA-*b*-PVOH copolymer on the surface of γ-Fe_2O_3 NPs does not change drastically the relaxivity properties. Concerning the distance of minimum approach of the protons, the values of $2R_{NMR}$ (19.6 nm) are larger than the average diameters of the magnetic cores d_w (7.5 nm) obtained from TEM technique. However, they remain well below the D_h values (120 nm), similarly to the work reported by Sander.[52]

To validate our findings in relaxivity studies of the γ-Fe_2O_3@PAA-*b*-PVOH NPs as potential MRI contrast agents, T_1 and T_2 values were measured at different frequencies. T_1 was 32.6 ms at 20 MHz and 85.7 ms at 60 MHz, while T_2 was 4.35 ms at 20 MHz and 4.66 ms at 60 MHz. We also collected the MRI images at 7 T on Bruker Pharmascan 70:16. T_2-weighted MR images of the γ-Fe_2O_3@PAA-*b*-PVOH NPs are shown (right side of each images) in Fig. 5b-1 at echo time of 10.1 ms and Fig. 5b-2 at echo time of 30.3 ms. PAA-*b*-PVOH copolymer solution with the sample concentration was taken as the blank (left side of each image). Due to the small T_2 value, the signal disappeared completely when the echo time reached 30.3 ms, while a slight change was observed for the blank, showing a significant negative contrast enhancement (signal darkening). In the T_1-weighted MR images of the γ-Fe_2O_3@PAA-*b*-PVOH NPs in Fig. 5b-3 (TR = 5000 ms) and Fig. 5b-4 (TR = 800 ms), compared with the blank, difference in the brightness of the γ-Fe_2O_3@PAA-*b*-PVOH NPs could also been obviously observed at different recovery times. Therefore, these results suggest that the γ-Fe_2O_3@PAA-*b*-PVOH NPs possess a potential application as MRI contrast agents, but also possibly for tracing *in vivo* fate of these nanoparticles when used as DDS, which will be discussed in the following section.

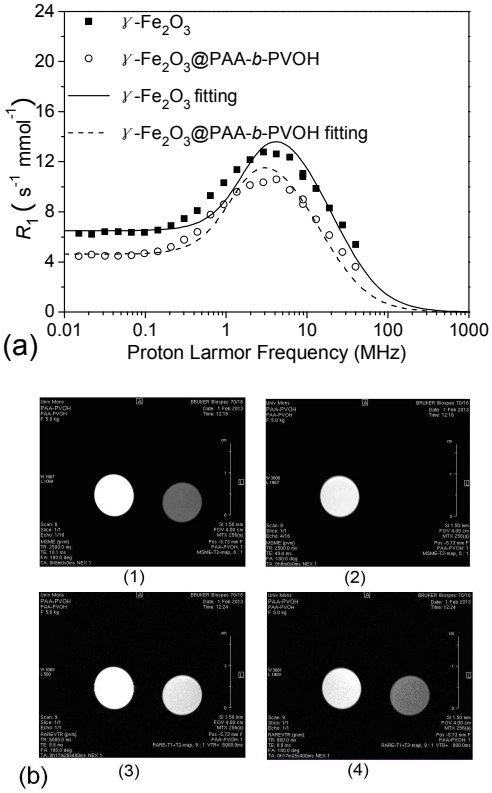

Fig. 5 (a) NMRD profiles of bare γ-Fe_2O_3 and γ-Fe_2O_3@PAA-*b*-PVOH NPs, and the parameters for the fitting of bare γ-Fe_2O_3 NPs are: $\tau_{Néel}$ = 4.0 ns, M_s = 21.7 Am^2/kg, D_{NMR} = 8.0 nm, while for γ-Fe_2O_3@PAA-*b*-PVOH NPs: $\tau_{Néel}$ = 3.7 ns, M_s = 16.8 Am^2/kg, D_{NMR} = 9.8 nm; (b) T_2-weighted MR images of the γ-Fe_2O_3@PAA-*b*-PVOH NPs aqueous suspension (right side of each images, 0.2 mM) and PAA-*b*-PVOH copolymer aqueous solution (left side of each images, 2.5 mg/L) at echo times equal to 10.1 ms (b-1) and 30.3 ms (b-2); and T_1-weighted MR images of the γ-Fe_2O_3@PAA-*b*-PVOH NPs aqueous suspension and PAA-*b*-PVOH copolymer aqueous solution at TR = 5000 ms (b-3) and TR= 800 ms (b-4) (echo time = 8.8 ms).

Capability of drug loading and release profiles of the γ-Fe_2O_3@PAA-*b*-PVOH NPs

A hydrophilic and positively-charged model drug, methylene blue (MB), was utilized to test the capability of drug loading and release profiles under different conditions of the as-prepared γ-Fe_2O_3@PAA-*b*-PVOH NPs for DDS application. Here, MB was loaded to the PAA-*b*-PVOH polymer corona through the electrostatic interaction between positively-charged MB and negatively-charged carboxylate groups of the deprotonated PAA blocks at pH 7.4 (Scheme 1). The presence of loaded MB was confirmed by UV/*vis* spectra of the MB-loaded γ-Fe_2O_3@PAA-*b*-PVOH NPs suspension (See ESI, Fig. S8†). The amount of loaded MB was determined spectrophotometrically, and a drug loading capacity (DLC) of 3.7 *wt*.% and drug loading efficiency (DLE) of 18.4 *wt*.% were estimated, comparable to those of others organic/inorganic nanoparticles aimed for DDS.[16,17,46] And the relatively low loading capacity might also be attributed to the low polymer fraction. Small decrease in D_h (107 nm) and ζ (-18 mV) for the MB-loaded γ-Fe_2O_3@PAA-*b*-PVOH NPs was observed (See ESI, Fig. S4b†), compared to 120 nm and -35 mV before loading. This might be due to the reduced charge density

View Article Online
DOI: 10.1039/C3NR02861E

on the PAA block in the presence of MB, in agreement with the results of the IS-responsive properties (Fig. 3b) and the report on DDS made of magnetic mesoporous silica nanoparticles coated with poly(*N*-isopropylacrylamide-*co*-methacrylic acid).[53]

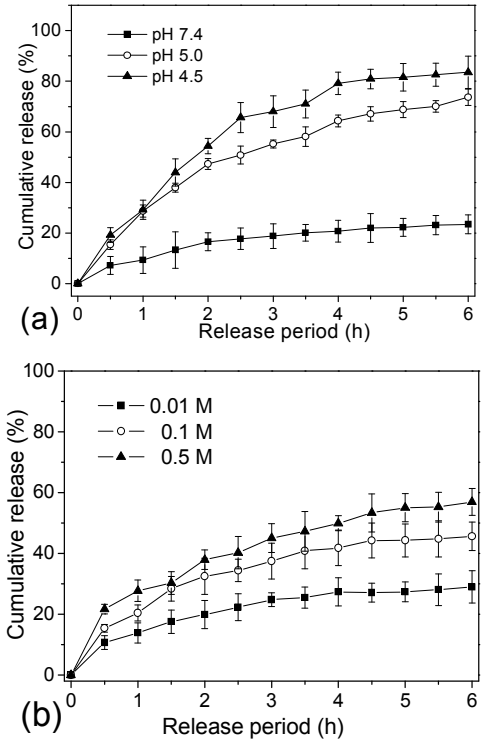

Fig. 6 (a) Cumulative release profiles of the MB-loaded γ-Fe_2O_3@PAA-*b*-PVOH NPs at 37ºC in buffers (10 mM) at different pH values and (b) cumulative release profiles at 37ºC in PBS buffer solutions (pH 7.4) with different C_{NaCl} (the solid lines just serve to guide the eye, and the bar graphs of each release profiles represent mean values ± standard deviation from three independent replicates).

As already discussed, the PAA-*b*-PVOH polymer coating are pH-responsive, thus variation in pH might be a route to trigger the release of loaded drugs. Fig. 6a showed the release profile at 37ºC under different pH conditions using some simulated physiological body fluids. While PBS buffer (10 mM, pH 7.4) is an isosmotic solution for cells, NaAc/HCl buffer (pH 4.5, 10 mM) can simulate some tumour acidic environment, NaAc/HCl buffer (pH 5.0, 10 mM) acidic environment of the lysosomes. Relatively slow release at pH 7.4 was observed due to the diffusion-controlled mechanism and a significantly faster release was detected at pH 5.0 (*ca*. 65% in 4 h), while release of *ca*. 78% was achieved in 4 h at pH 4.5. Here, this pH-triggered release could still be explained by the protonation of carboxylic groups of PAA blocks upon decrease in pH, consequently leading to the dissociation of the carboxylate/MB adducts. Moreover, shrinkage of the polymer coating, as discussed in the former section, may also contribute to a higher diffusion coefficient.

As reported by Meszaros *et al.*,[23] no desorption was observed for the previously-adsorbed polyelectrolyte [poly(ethyleneimine), PEI, IEP of 10.5] from silica surface, when the pH was decreased from 9.5 to 5.8. Although this pH change resulted a significant increase in the bulk charge density of PEI (30%), desorption PEI chains was still significantly hindered, since this high activation energy for PEI desorption from the silica surface was thought to be non-Coulomb affinity. Therefore, it is plausible to conjecture that the polymer corona might be still immobilized on the γ-Fe_2O_3 core during the endocytosis process, when pH decreases from 7.4 to 5.0, and partial PAA segments are supposed to be protonated. For other more acidic or basic condition, the immobilized polymer coating is envisaged to be desorbed due to the reduced electrostatic interaction, which will be discussed in a forthcoming paper. While in the pH of 7.4 ~ 5.0, we believed that the polymer coating should be stable enough to stabilize the nanoparticles.

Due to the dependence of chain conformation of the polyelectrolyte on IS, variation in IS has also been utilized as a stimulus to trigger the drug release, and some studies on IS-triggered release were previously reported.[19,24,25] The release behaviours in PBS buffer (pH 7.4) with C_{NaCl} (0.01, 0.1 and 0.5 M) at 37ºC are summarized in Fig. 6b. As expected, a faster release could be detected at higher C_{NaCl}. Satu [54] explained the IS-triggered release mechanism by the ion exchange of the uploaded drugs by the free ions in the release medium. Herein, a synergetic contribution of both ion exchange and conformation change are expected to contribute to the IS-triggered release.

Generally, ionic strength might post a double effect on the adsorption of polyelectrolytes.[22] Since the salt screens the repulsion of equal charges the NPs surface and of the polyelectrolyte molecules, resulting in an increase in the degree of dissociation of the polyelectrolyte molecules. But at the same time, the salt also screens the attractive interactions between the positive surface and the negative polyelectrolyte molecules. Thus, if a polyelectrolyte is adsorbed on oppositely charged surfaces mainly by electrostatic interaction, the adsorbed amount should decrease with increasing salt concentration. On the other hand, if the adsorbed amount increases with increasing salt concentration, one can postulate that there are specific non-electrostatic interactions between the surface and the molecules. As reported by Lewandowski and coll.,[22] an IS increase from 0.01 M to 1 M could result in doubled PAA absorbed amount onto aluminium oxide particles at pH 5.2. Thus it can be conjectured that within the intracellular counterpart, such as endosome (pH 5.5~6.0) or lysosomes (pH 5.0), increase in IS will not cause desorption of the pre-immobilized polymer coating. While according to the report on other systems, such as Poptoshev's report[55] on adsorption of poly(ethylene oxide) monomethyl ether methacrylate and methacryloxyethyl trimethylammonium chloride (PEOMEMA:METAC) onto silica particles at pH 6.0, increase in $NaNO_3$ concentration from 0.1 mM to 100 mM could induce an desorption of *ca.* 30% of the formerly-attached polymers. Thus we might infer that part of the previously-absorbed PAA-*b*-PVOH copolymer would be detached, and the remained. Desorption of the polymer coating, stability of the maghemite NPs upon increase in IS would be discussed in detailed in a forthcoming report.

View Article Online
DOI: 10.1039/C3NR02861E

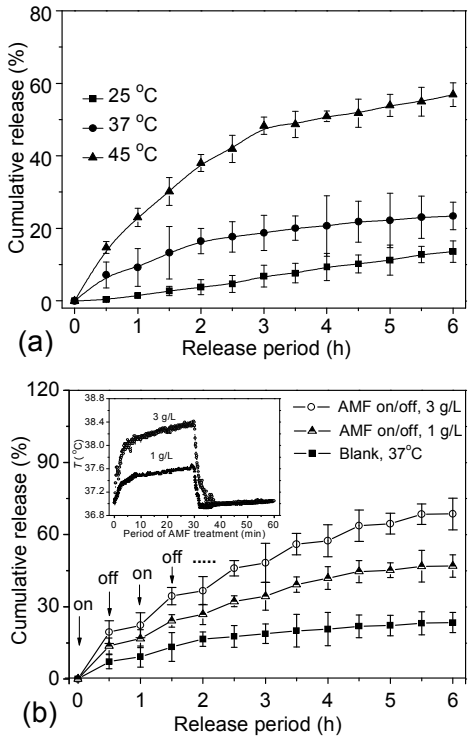

Fig. 7 (a) Cumulative release profiles of MB from the MB-loaded γ-Fe_2O_3@PAA-*b*-PVOH NPs suspension in PBS buffer solution (pH 7.4, 10 mM) at different temperatures; (b) release profiles under multiple AMF on/off cycles of the MB-loaded γ-Fe_2O_3@PAA-*b*-PVOH aqueous suspension at 3 g/L and 1 g/L (37ºC, pH 7.4), while release without AMF treatment (3 g/L, 37ºC, pH 7.4) was taken as a blank, and inset: evolution of temperature of the release medium during AMF on/off treatment for the MB-loaded γ-Fe_2O_3@PAA-*b*-PVOH suspension at 3 g/L and 1 g/L, (the solid lines just serve to guide the eye, and the bar graphs of each release profiles represent mean values ± standard deviation from three independent replicates).

There are many reports studying on thermo-triggered release from nanoparticles with thermo-responsive polymer corona.[17,26,56] Here, even though PAA-*b*-PVOH copolymer is not reputed to be sensitive to temperature, the electrostatic binding between the carboxylic groups and MB molecules might still show some dependence on temperature. Because of the thermodynamically electrostatic binding, an increase in temperature may lead to the dissociation of the electrostatic interactions,[57] thus a positive temperature-dependent release is expected. Fig. 7a summarizes the release profiles at 25ºC (storage), 37ºC (delivery) and 45ºC (hyperthermia therapy), and faster release was observed under higher temperature, in line with the thermodynamically-dependent binding between the MB molecules and deprotonated PAA blocks.

Furthermore, due to the heating capability of γ-Fe_2O_3@PAA-*b*-PVOH NPs under AMF application (Fig. 4), AMF-induced local heating might also be an elegant way to trigger the release. To confirm this hypothesis, remotely AMF-triggered release behaviours were studied by applying AMF with the home-designed release apparatus (Fig. 1). The MB-loaded γ-Fe_2O_3@PAA-*b*-PVOH NPs suspension was dialyzed against PBS buffer (10 mM, pH 7.4), and a 37ºC water bath was circulating during the experiments to mimic physiological conditions. The release behaviours were followed under multiple AMF on/off cycles with an interval of 30 min, while release without AMF was taken as a blank (Fig. 7b). Comparing with the release at 37ºC without AMF, a faster release was observed after AMF application, and the AMF-triggered release was also directly dependent on the NPs concentration. Thus, AMF is a convenient route to control the on-demand drug release. Additionally, the temperature evolution of the release medium was also followed with a thermo-sensor (Fig. 7b-inset). As observed, the temperature reached a plateau in a few minutes upon the application of AMF. However, when AMF was removed, the temperature rapidly decreased to the initial temperature. It is deserved to note that, magnetic hyperthermia therapy is always doubted due to some side-effect risks, such as overheating.[7,8] Here, a mild heating in the release medium was observed (less than 2ºC), suggesting that less side effects would be brought up to the biological tissue nearby, if used *in vivo*, during the AMF-triggered release.

Preliminary studies on cytotoxicity and cellular uptake of the γ-Fe_2O_3@PAA-*b*-PVOH NPs

To explore the potential for biomedical application, cytotoxicity of diverse inorganic nanoparticles has been investigated against different cell lines. Some of those studies showed that cell proliferation or cellular adhesion ability was significantly quenched after incubation with nanoparticles such as carbon nanotubes,[58] iron oxides or their derivatives[59, 60] and other metals or metal oxides nanoparticles.[61] At cytotoxic dose levels, cellular apoptosis or cell cycle arrest was observed upon directly exposure to silica,[62] CNTs[58] and iron oxide.[63] Furthermore, most inorganic nanoparticles are known to be rapidly taken up by spleen and liver, mainly by the macrophages, rendering their half-lives in the circulation very short.[64,65] An optimal surface modification becomes necessary for those nanoparticles to be applied as DDS, in order to achieve a prolonged plasma half-life as well as improved biocompatibility and colloidal stability under hydrophilic or lipophilic conditions. Up to now, there are many reports on polymer-based surface modification,[6,73] such as poly(ethylene glycol),[66,67] poly(vinyl alcohol),[68,69] poly(acrylic acid),[70] polypeptide,[71] polyvinylpyrrolidone,[72] *etc*. These kinds of surface modified inorganic nanoparticles with optimal size, appropriate antifouling surface and good stability can remain within the vasculature for a long period. Moreover, they accumulate in the specifically-desirable sites via the well-established enhanced permeation and retention (EPR) effect, which might maximize their performance in targeted biomedical imaging and also drug delivery.[18,74]

After surface coating, the γ-Fe_2O_3@PAA-*b*-PVOH NPs were supposed to exhibit decreased cytotoxicity as potential DDS. To verify this, the *in vitro* differential cytotoxicity assessment against fibroblasts-like L929 cell line was carried out via the MTS assay. Cell viabilities were presented as the ratio of the living cell number after treatment to that of the control (non-treated cells). Fig. 8a and 8b show the cell viabilities of L929 cells after incubation with the bare γ-Fe_2O_3 NPs or γ-Fe_2O_3@PAA-*b*-PVOH NPs at different concentrations in 24 and 48 h, respectively. It is noticeable that a higher cell viability with

View Article Online
DOI: 10.1039/C3NR02861E

less cytotoxicity was observed for the γ-Fe_2O_3@PAA-*b*-PVOH NPs compared to the bare γ-Fe_2O_3 NPs, due to the presence of PAA-*b*-PVOH copolymer on the surface.

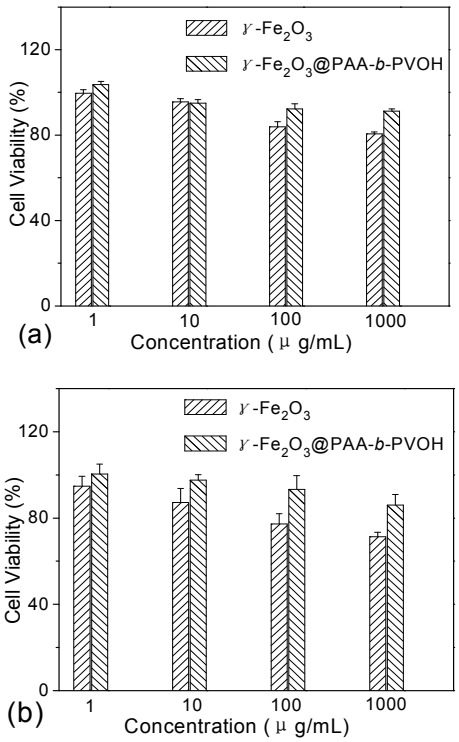

Fig. 8 Cytotoxicity profiles of the bare γ-Fe_2O_3 NPs and γ-Fe_2O_3@PAA-*b*-PVOH NPs against the fibroblasts-like L929 cells determined via MTS assay at different concentrations after 24-h (a) and 48-h incubation (b), respectively. Percentage viabilities of the L929 cells were expressed relative to the untreated cells (control) and results were presented as mean values ± standard deviation from five independent samples.

For the application of DDS, cellular uptake of those nano-vehicles will directly reflect the delivery efficiency and *in vivo* bio-availability. Herein, preliminary cell uptake studies were carried out with a model cancer cell, human melanoma MEL-5 cell line. First, fluoresceinamine (FA) was used as a convenient fluorescence probe to label the γ-Fe_2O_3@PAA-*b*-PVOH NPs, owing to its accessible excitation and emission wavelengths (*Ex*: 488 nm and *Em*: 525 nm). For the PAA-*b*-PVOH copolymer, FA groups were easily grafted to the PAA blocks via amidation reaction with a grafting degree of *ca*. 1.4 *mol*.% (AA-FA monomer units out of overall AA monomer units) as confirmed from ^{1}H NMR analysis (See ESI, Fig. S1†). Presence of FA groups in the FA-labelled γ-Fe_2O_3@PAA-*b*-PVOH was also confirmed by UV/*vis* spectroscopy (See ESI, Fig. S8†). Usually, DNA in the nuclei is the primary target of various anticancer drugs, for examples, doxorubicin and cisplatin.[75] Therefore, it is of significance to study the *in vivo* fate of those nano-vehicles as DDS for anti-cancer drugs.

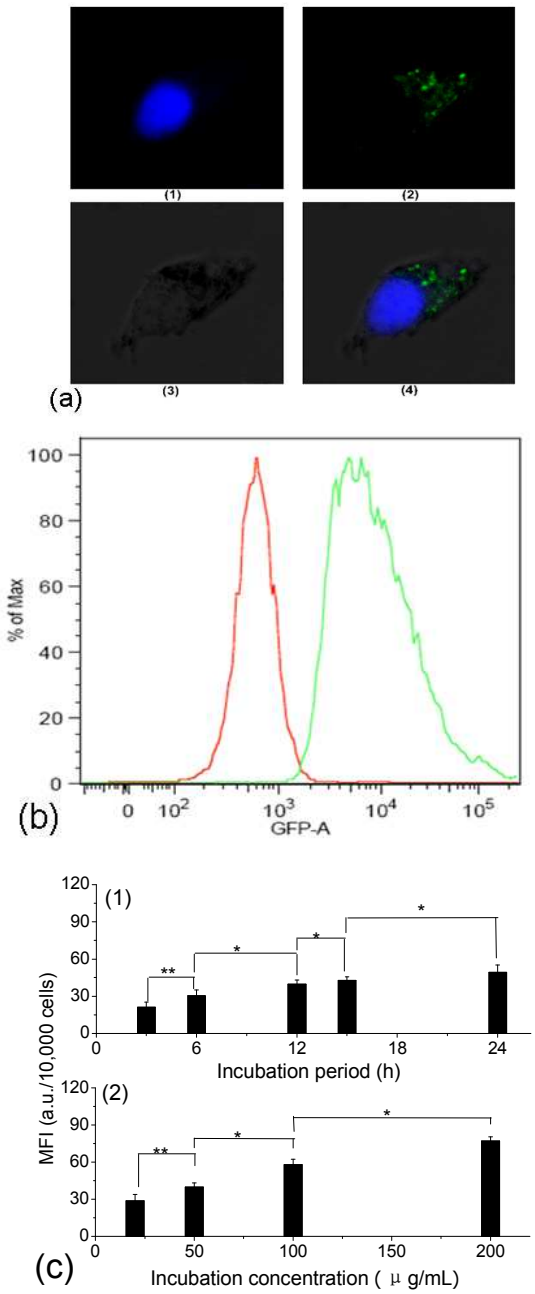

Fig. 9 (a) CLSM images of the MEL-5 cells after 12-h incubation with the FA-labeled γ-Fe_2O_3@PAA-*b*-PVOH NPs (50 μg/mL): (1) DAPI (blue), (2) FITC (green), (3) phase contrast pattern, and (4) merged images; (b) FACS histogram of untreated MEL-5 cells (red) and treated cells after 12-h incubation with the FA-labelled γ-Fe_2O_3@PAA-*b*-PVOH NPs (50 μg/mL, green), with the log of FITC intensity (GFP-A on *x*-axis) plotting against the number of cells (% of Max on *y*-axis), and (d) dependence of the mean fluorescence intensity (MFI) of the treated MEL-5 cells on the incubation period (50 μg/mL) (c-1) and concentration (12-h incubation) (c-2) for the FA-labelled γ-Fe_2O_3@PAA-*b*-PVOH NPs (* = $P < 0.05$, ** = $P < 0.01$ by the Student' *t*-test, error bars of each graph represented standard deviation from three independent samples).

Herein, confocal laser scanning microscopy (CLSM) was used to qualitatively monitor the distribution of γ-Fe_2O_3@PAA-*b*-PVOH NPs (Fig. 9a). Blue and green fluorescence channels referred the DAPI stained nuclei (Fig. 9a-1) and the internalized FA-labelled γ-Fe_2O_3@PAA-*b*-PVOH NPs (Fig. 9a-2),

View Article Online
DOI: 10.1039/C3NR02861E

respectively. These internalized nanoparticles could be observed in the phase contrast pattern (Fig. 9a-3). Merging of the three images (Fig. 9a-4) evidences the accumulation of γ-Fe_2O_3@PAA-*b*-PVOH NPs within the cytoplasm. The cellular uptake from CLSM observation was further studied by using fluorescence-activated cell sorter (FACS) measurement. As shown in Fig. 9b, after 12-h incubation with FA-labelled γ-Fe_2O_3@PAA-*b*-PVOH NPs (50 μg/mL), a totally different cell population was detected, evidencing by the sharp shift in the histogram of *Counts vs*. *GFP-A*, and nearly 100% of the cells were internalized with the γ-Fe_2O_3@PAA-*b*-PVOH NPs.

Furthermore, to further analyze the cellular uptake, we performed quantitative analyses of the FACS results. The ratio of fluorescence intensity of 10,000 treated cells to that of 10,000 untreated cells was expressed as mean fluorescence intensity (MFI), which was taken to evaluate the cellular uptake amount. Incubation in different periods (3, 6, 12, 15 and 24 h) with a fixed incubation concentration (50 μg/mL) was performed to study the uptake kinetics (Fig. 9c-1). Nearly 100% of the MEL-5 cells were positively internalized with the FA-labelled γ-Fe_2O_3@PAA-*b*-PVOH (50 μg/mL) NPs after 3-h incubation (See ESI, Fig. S9†). MFI increased very quickly during the first 12 h and the internalization process slowed down afterwards. This indicates that γ-Fe_2O_3@PAA-*b*-PVOH NPs could be readily internalized into the MEL-5 cells within a relatively short period of time. Moreover, dose-dependent cellular uptake behaviour of the γ-Fe_2O_3@PAA-*b*-PVOH NPs into MEL-5 cancer cells was also evidenced in Fig. 9c-2.

Due to the limitation of CLSM in discerning individual nanoparticles after internalization, the treated MEL-5 cells were fixed and then sliced for TEM observation, in order to explore the cellular uptake mechanism of the γ-Fe_2O_3@PAA-*b*-PVOH NPs. Generally, entering of NPs within cellular counterparts is known to be strongly dependent on their physicochemical properties, *e.g.* size, shape, surface properties, *etc*. Particularly, the surface properties, such as surface materials and surface charges, are known to be one of the essential factors that directly decide the cellular uptake, since NPs would interact with those complex biological environments prior to the cellular systems.[76] As reported by Gupta,[77] the uncoated magnetic nanoparticles could internalize within the cell cytoplasm, but caused disruption of the cell membrane and disorganized cell cytoskeleton. However, after surface PEG-modification, the cellular uptake increased greatly in comparison to that of un-modified NPs, and clusters were formed within the lysosomes, without changing the cytoskeleton of fibroblasts. In our case of γ-Fe_2O_3@PAA-*b*-PVOH NPs, due to the presence of PVOH external corona, the NPs are expected to internalize within the MEL-5 cells without affecting the cytoskeleton, which was evidenced in Fig. 10a. The NPs, in the form of clusters and appearing as black dots (marked with arrows), were observed within the cell cytoplasm but not in the nuclei. Moreover, it revealed that the γ-Fe_2O_3@PAA-*b*-PVOH NPs accumulated within the MEL-5 cells in large phagosomes, which might be phagolysosomes (Fig. 10a-inset).

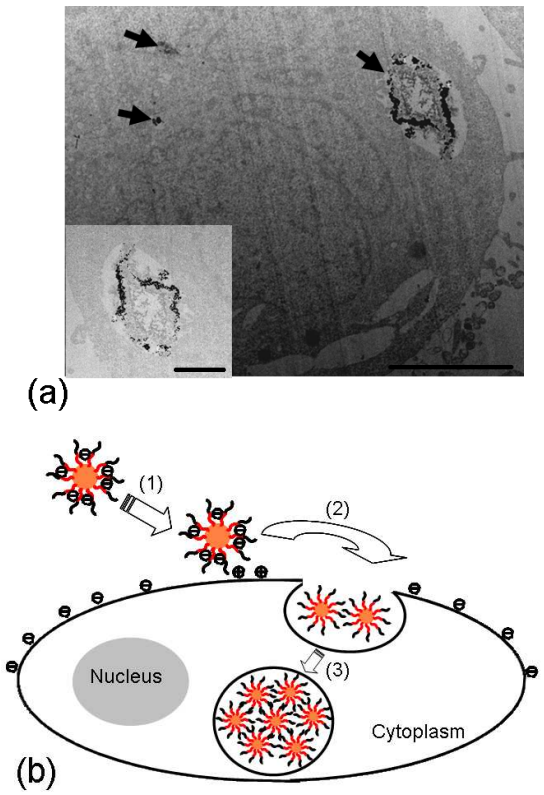

Fig. 10 (a) Representative TEM image of the treated MEL-5 cells (scale bar: 5 μm), and inset: partially-magnified image (scale bar: 1 μm); (b) mechanism of cellular uptake of the γ-Fe_2O_3@PAA-*b*-PVOH NPs within melanoma MEL-5 cells, (b-1): nonspecific binding and clustering of the maghemite NPs on cationic sites of the plasma membrane, (b-2): clathrin-mediated endocytosis of the maghemite NPs within early endosomes in the form of clusters, and (b-3): accumulation of maghemite NPs within the phagolysosomes.

As previously reported by Harush-Frenkel,[78,79] surface charges of magnetic NPs affect not only their internalization ability, but also the underlying cellular endocytosis mechanism. In their study, both cationic and anionic nanoparticles were internalized mainly to the clathrin-mediated endocytic machinery, and a fraction of both NPs formulations was suspected to internalize through a macropinocytosis-dependent pathway. Moreover, positively charged NPs were internalized rapidly with a higher accumulation amount. Negatively charged NPs showed an inferior rate of endocytosis and utilized the clathrin-mediated endocytosis pathway less. Wilhelm and Gazeau[80] reported that anionic magnetic NPs exhibited a high level of internalization by interacting strongly and nonspecifically with the plasma membrane. The internalization of these negatively-charged NPs was explained by the nonspecific binding and clustering of the NPs on cationic sites of the plasma membrane (relatively scarcer than negatively-charged domains) and the subsequent endocytosis process. Magnetic NPs stabilized by carboxyl-functionalized 3rd generation poly(amidoamine) dendrimers[81] were also reported to be easily taken up into human epithelial carcinoma cells, presumably either through pinocytosis process. In our case, due to the presence of PVOH external corona, γ-Fe_2O_3@PAA-*b*-PVOH NPs are expected to internalize within the MEL-5 cells without affecting the cytoskeleton, which was evidenced in Fig. 10a. Moreover, due to the negatively-charged surface, the

View Article Online
DOI: 10.1039/C3NR02861E

internalized rate must be slower than other positively-charged NPs with similar size and components. However, Fink and coll.[82] revealed that the zeta potential of all three different surface-charged (positive, negative, neutral) PVA-coated magnetic NPs was found to be around -12 mV after incubation in the FBS supplemented cell culture medium (followed by magnetic separation and re-dispersions in water), irrespective of their initial surface potentials. While the higher uptake of positively-charged NPs within HeLa cells compared to the negatively- and neutrally-charged NPs could be explained by sedimentation of larger NPs or agglomerates in the cell culture plate, due to the lower colloidal stability. Thus, based on these reports, the uptake of γ-Fe_2O_3@PAA-*b*-PVOH NPs might still be explained by the initial non-specifically binding and clustering of the NPs on the cationic sites of the plasma membrane,[80] the following clathrin-mediated endocytosis process,[77] and finally accumulation within the phagolysosomes, as shown in Fig. 10b. Further experiments might be needed to have clearer insights on the cellular fate of the γ-Fe_2O_3@PAA-*b*-PVOH NPs within the MEL-5 cells. It deserves to note that, the accumulation of γ-Fe_2O_3@PAA-*b*-PVOH NPs as clusters within the proposed phagolysosomes, when they enter the MEL-5 cells, should be in favour of the subsequent MR imaging, if biomedical image are needed to follow the *in vivo* fate of these DDS or diagnose the disease sites, *etc*.

Conclusions

In this work, stimuli-responsive magnetic nanoparticles composed of γ-Fe_2O_3 cores and PAA-*b*-PVOH corona were prepared. They exhibited responsiveness to external variations in pH and ionic strength. Because of the presence of pH-insensitive PVOH block, the nanoparticles were stable even at lower pH values around the p*K*a of PAA block. Local heating was generated under alternative magnetic field, with a normalized SHP of 25 W/(g Fe), due to the superparamagnetic properties of the γ-Fe_2O_3@PAA-*b*-PVOH NPs. A model drug, methylene blue, was loaded into the polymer corona (DLC 3.7 *wt*.% and DLE 18.4 *wt*.%), and variation in pH, IS or temperature could be utilized as stimuli to trigger the drug release in buffer solutions. Faster release under AMF treatment was also observed with a mild heating over the release medium. The possibility to remotely magnetically-trigger the drug release was demonstrated. Cytotoxicity against L929 cell line showed that γ-Fe_2O_3@PAA-*b*-PVOH NPs exhibited an improved biocompatibility due to the presence of PVOH blocks. Furthermore, incubation time- and concentration-dependent cellular uptake behaviours were also evidenced. Moreover, the presence of the superparamagnetic γ-Fe_2O_3 core also allows tracing the DDS *in vivo* by using the MRI technique. In the light of this study, the PAA-*b*-PVOH coated magnetic γ-Fe_2O_3 particles represent a promising opportunity for the development of clinically relevant and remotely AMF-triggered theranostic modalities.

Acknowledgements

The authors thank the Belgian National Funds for Scientific Research (F.R.S.-FNRS), the European Community in the frame of the Erasmus Mundus International doctoral school IDS-FunMat and the Science Policy Office of the Belgian Federal Government (PAI VII-05) for their financial support. The authors are also grateful to Prof. Sébastien Lecommandoux and Dr Olivier Sandre for the access to the magnetic hyperthermia setup at the Laboratoire de Chimie des Polymères Organiques, University of Bordeaux. The authors are also grateful to the GIGA-imaging and flowcytometry platform in University of Liège for their help with CLSM and flowcytometry measurement. L.V.E and S.L. would like to thank FNRS, ARC and ENCITE programs for financial support.

Notes and references

[a] *Center for Education and Research on Macromolecules (CERM), University of Liège, B6a Sart-Tilman, B-4000 Liège, Belgium. Fax: (32)4-36663497; Tel: (32)4-3663565; E-mail: christophe.detrembleur@ulg.ac.be, c.jerome@ulg.ac.be*
[b] *Laboratory of Mammalian Cell Culture (GIGA-R), University of Liège, B6 Sart Tilman, B-4000 Liège, Belgium.*
[c] *CNRS, Univ. Bordeaux, ICMCB, UPR 9048, F-33600 Pessac, France. Fax: +33 540 002 761; Tel: +33 540 002 651; E-mail: duguet@icmcb-bordeaux.cnrs.fr*
[d] *Department of General, Organic & Biomedical Chemistry, NMR & Molecular Imaging Laboratory, University of Mons, Avenue Maistriau, 19, B-7000 Mons, Belgium.*
[e] *CeCaMa, Univ. Bordeaux, ICMCB, F-33600 Pessac, France.*

† Electronic Supplementary Information (ESI) available: ^{1}H NMR spectra, XRD pattern, XPS spectra, magnetization curves, TEM image, UV/vis spectra, TGA curves of the nanoparticles or copolymers, calibration curve of MB concentration and FACS histogram of the treated cells, *etc*. See DOI: 10.1039/b000000x/

1. H. A. Klok, A. Rosler and G. W. M. Vandermeulen, *Adv Drug Deliver Rev*, 2001, **53**, 95-108.
2. K. Kataoka, A. Harada and Y. Nagasaki, *Adv Drug Deliver Rev*, 2001, **47**, 113-131.
3. S. Ganta, H. Devalapally, A. Shahiwala and M. Amiji, *J Control Release*, 2008, **126**, 187-204.
4. L. E. Strong and J. L. West, *Wiley Interdiscip Rev Nanomed Nanobiotechnol*, 2011, **3**, 307-317.
5. N. A. Frey, S. Peng, K. Cheng and S. Sun, *Chem Soc Rev*, 2009, **38**, 2532-2542.
6. M. Mahmoudi, S. Sant, B. Wang, S. Laurent and T. Sen, *Adv Drug Deliv Rev*, 2011, **63**, 24-46.
7. E. Duguet, S. Vasseur, S. Mornet and J. M. Devoisselle, *Nanomedicine*, 2006, **1**, 157-168.
8. S. Mornet, S. Vasseur, F. Grasset, P. Veverka, G. Goglio, A. Demourgues, J. Portier, E. Pollert and E. Duguet, *Prog Solid State Chem*, 2006, **34**, 237-247.
9. S. Mornet, S. Vasseur, F. Grasset and E. Duguet, *J Mater Chem*, 2004, **14**, 2161-2175.
10. F. M. Martin-Saavedra, E. Ruiz-Hernandez, A. Bore, D. Arcos, M. Vallet-Regi and N. Vilaboa, *Acta Biomater*, 2010, **6**, 4522-4531.
11. A. Baeza, E. Guisasola, E. Ruiz-Hernandez and M. Vallet-Regi, *Chem Mater*, 2012, **24**, 517-524.
12. S. Louguet, B. Rousseau, R. Epherre, N. Guidolin, S. Mornet, E. Duguet, S. Lecommandoux and C. Schatz, *Polymer Chemistry*, 2012, **3**, 1408-1417.
13. B. Julian-Lopez, C. Boissiere, C. Chaneac, D. Grosso, S. n. Vasseur, S. Miraux, E. Duguet and C. Sanchez, *J Mater Chem*, 2007, **17**, 1563-1569.
14. B. Haley and E. Frenkel, *Urol Oncol*, 2008, **26**, 57-64.
15. J. Gao, W. Zhang, P. Huang, B. Zhang, X. Zhang and B. Xu, *J Am Chem Soc*, 2008, **130**, 3710-3711.
16. M. Guo, C. Que, C. Wang, X. Liu, H. Yan and K. Liu, *Biomaterials*, 2011, **32**, 185-194.
17. M. F. Ma, K. Y. Wu, J. Tang, D. Li, C. Wei, J. Guo, S. J. Wang and C. C. Wang, *J Mater Chem*, 2012, **22**, 15206-15214.
18. J. Gao, H. Gu and B. Xu, *Acc Chem Res*, 2009, **42**, 1097-1107.

View Article Online
DOI: 10.1039/C3NR02861E

19. S. Ghosh, H. Mashayekhi, P. Bhowmik and B. Xing, *Langmuir*, 2010, **26**, 873-879.
20. A. Debuigne, J. Warnant, R. Jerome, I. Voets, A. de Keizer, M. A. Stuart and C. Detrembleur, *Macromolecules*, 2008, **41**, 2353-2360.
21. S. Ghosh, W. Jiang, J. D. McClements and B. Xing, *Langmuir*, 2011, **27**, 8036-8043.
22. K. Vermohlen, H. Lewandowski, H. D. Narres and M. J. Schwuger, *Colloids Surf A Physicochem Eng Asp*, 2000, **163**, 45-53.
23. R. Meszaros, I. Varga and T. Gilanyi, Langmuir, 2004, 20, 5026-5029.
24. Y. Zhu, J. Shi, W. Shen, X. Dong, J. Feng, M. Ruan and Y. Li, *Angew Chem Int Ed Engl*, 2005, **44**, 5083-5087.
25. L. Han, Z. Mao, H. Wuliyasu, J. Wu, X. Gong, Y. Yang and C. Gao, *Langmuir*, 2012, **28**, 193-199.
26. M. Karg, Y. Lu, E. Carbo-Argibay, I. Pastoriza-Santos, J. Perez-Juste, L. M. Liz-Marzan and T. Hellweg, *Langmuir*, 2009, **25**, 3163-3167.
27. M. Lattuada and T. A. Hatton, *Langmuir*, 2007, **23**, 2158-2168.
28. A. Aqil, S. Vasseur, E. Duguet, C. Passirani, J. P. Benoît, R. Jérôme and C. Jérôme, *J Mater Chem*, 2008, **18**, 3352-3360.
29. T. Y. Liu, S. H. Hu, T. Y. Liu, D. M. Liu and S. Y. Chen, *Langmuir*, 2006, **22**, 5974-5978.
30. A. Aqil, C. Detrembleur, B. Gilbert, R. Jérôme and C. Jérôme, *Chem Mater*, 2007, **19**, 2150–2154.
31. D. Suzuki, S. Tsuji and H. Kawaguchi, *J Am Chem Soc*, 2007, **129**, 8088-8089.
32. T. Isojima, M. Lattuada, J. B. Vander Sande and T. A. Hatton, *ACS nano*, 2008, **2**, 1799-1806.
33. S.W. Song, K. Hidajat, and S. Kawi, *Chem Comm*, 2007, **42**, 4396-4398.
34. Q. Gao, Y. Xu, D. Wu, Y. Sun and X. Li, *J Phys Chem C*, 2009, **113**, 12753–12758.
35. Q. He, Z. Zhang, F. Gao, Y. Li and J. Shi, *Small*, 2011, **7**, 271-280.
36. J. Panyam and V. Labhasetwar, *Adv Drug Deliv Rev*, 2003, **55**, 329-347.
37. D. R. Lynch and S. H. Snyder, *Ann Rev Biochem*, 1986, **55**, 773-799.
38. J. C. Grunlan, L. Liu and Y. S. Kim, *Nano Lett*, 2006, **6**, 911-915.
39. D. X. Li, Q. He, Y. Cui and J. B. Li, *Chem Mater*, 2007, **19**, 412-317.
40. R. Massart, *IEEE Trans Magn*, 1981, **17**, 1247-1248.
41. S. W. Cao, Y. J. Zhu, M. Y. Ma, L. Li and L. Zhang, *J Phys Chem C*, 2008, **112**, 1851-1856.
42. S. Louguet, A. C. Kumar, G. Sigaud, E. Duguet, S. Lecommandoux and C. Schatz, *J Colloid Interface Sci*, 2011, **359**, 413-422.
43. K. Hayashi, K. Ono, H. Suzuki, M. Sawada, M. Moriya, W. Sakamoto and T. Yogo, *Acs Appl Mater Inter*, 2010, **2**, 1903-1911.
44. S. S. Huang, Y. Fan, Z. Y. Cheng, D. Y. Kong, P. P. Yang, Z. W. Quan, C. M. Zhang and J. Lin, *J Phys Chem C*, 2009, **113**, 1775-1784.
45. C. Xu, B. B. Wayland, M. Fryd, K. I. Winey and R. J. Composto, *Macromolecules*, 2006, **39**, 6063-6070.
46. X. He, X. Wu, X. Cai, S. Lin, M. Xie, X. Zhu and D. Yan, *Langmuir*, 2012, **28**, 11929-11938.
47. L. R. Yang, C. Guo, L. W. Jia, K. Xie, Q. H. Shou and H. Z. Liu, *Ind Eng Chem Res*, 2010, **49**, 8518-8525.
48. L. L. Lao and R. V. Ramanujan, *J Mater Sci*, 2004, **15**, 1061-1064.
49. M. Ma, Y. Wu, J. Zhou, Y. K. Sun, Y. Zhang and N. Gu, *J Magn Magn Mater*, 2004, **268**, 33-39.
50. P. G. A, S. A. Doherty, C. A. Grimes, W. R. Seitz, W. Andra, C. G. d'Ambly, I. Hilger, W. A. Kaiser, U. Richter and H. G. Schmidt, *IEEE Trans Magn*, 1998, **34**, 3745-3754.
51. H. Sakurai, T. Sanji, Y. Nakatsuka and F. Kitayama, *Chem Commun*, 1999, 2201-2202.
52. P. Arosio, J. Thevenot, T. Orlando, F. Orsini, M. Corti, M. Mariani, L. Bordonali, C. Innocenti, C. Sangregorio, H. Oliveira, S. Lecommandoux, A. Lasciialfari and O. Sandre, *J Mater Chem B*, 2013.
53. B. S. Chang, X. Y. Sha, J. Guo, Y. F. Jiao, C. C. Wang and W. L. Yang, *J Mater Chem*, 2011, **21**, 9239-9247.
54. T. Tarvainen, B. Svarfvar, S. Akerman, J. Savolainen, M. Karhu, P. Paronen and K. Jarvinen, *Biomaterials*, 1999, **20**, 2177-2183.
55. J. Iruthayaraj, E. Poptoshev, A. Vareikis, R. das Makuska, A. van der Wal and P. M. Claesson, Macromolecules, 2005, 38, 6152-6160.
56. H. G. Tang, S. Shen, J. Guo, B. S. Chang, X. G. Jiang and W. L. Yang, *J Mater Chem*, 2012, **22**. 16095-16103.
57. K. Brandenburg, A. David, J. Howe, M. H. Koch, J. Andra and P. Garidel, *Biophys J*, 2005, **88**, 1845-1858.
58. S. K. Manna, S. Sarkar, J. Barr, K. Wise, E. V. Barrera, O. Jejelowo, A. C. Rice-Ficht and G. T. Ramesh, *Nano Lett*, 2005, **5**, 1676-1684.
59. C. C. Berry, S. Wells, S. Charles and A. S. Curtis, *Biomaterials*, 2003, **24**, 4551-4557.
60. T. R. Pisanic, 2nd, J. D. Blackwell, V. I. Shubayev, R. R. Finones and S. Jin, *Biomaterials*, 2007, **28**, 2572-2581.
61. S. M. Hussain, K. L. Hess, J. M. Gearhart, K. T. Geiss and J. J. Schlager, *Toxicol In Vitro*, 2005, **19**, 975-983.
62. M. J. McCabe, *Toxicol Sci*, 2003, **76**, 1-2.
63. C. C. Berry, S. Wells, S. Charles, G. Aitchison and A. S. Curtis, *Biomaterials*, 2004, **25**, 5405-5413.
64. S. D. Li and L. Huang, *Mol Pharm*, 2008, **5**, 496-504.
65. M. A. Dobrovolskaia and S. E. McNeil, *Nat Nanotechnol*, 2007, **2**, 469-478.
66. D. P. Lankveld, R. G. Rayavarapu, P. Krystek, A. G. Oomen, H. W. Verharen, T. G. van Leeuwen, W. H. De Jong and S. Manohar, *Nanomedicine*, 2011, **6**, 339-349.
67. S. D. Perrault, C. Walkey, T. Jennings, H. C. Fischer and W. C. Chan, *Nano Lett*, 2009, **9**, 1909-1915.
68. M. J. Roberts, M. D. Bentley and J. M. Harris, *Adv Drug Deliv Rev*, 2002, **54**, 459-476.
69. G. B. Shan, J. M. Xing, M. F. Luo, H. Z. Liu and J. Y. Chen, *Biotechnol Lett*, 2003, **25**, 1977-1981.
70. K. Burugapalli, V. Koul and A. K. Dinda, *J Biomed Mater Res A*, 2004, **68**, 210-218.
71. M. Lewin, N. Carlesso, C. H. Tung, X. W. Tang, D. Cory, D. T. Scadden and R. Weissleder, *Nat Biotechnol*, 2000, **18**, 410-414.
72. J. Huang, L. Bu, J. Xie, K. Chen, Z. Cheng, X. Li and X. Chen, *Acs Nano*, 2010, **4**, 7151-7160.
73. A. K. Gupta and M. Gupta, *Biomaterials*, 2005, **26**, 3995-4021.
74. V. I. Shubayev, T. R. Pisanic, 2nd and S. Jin, *Adv Drug Deliv Rev*, 2009, **61**, 467-477.
75. L. Rajendran, H. J. Knolker and K. Simons, *Nat Rev Drug Discov*, 2010, **9**, 29-42.
76. A. Verma and F. Stellacci, *Small*, 2010, **6**, 12-21.
77. A. K. Gupta and A. S. Curtis, *J Mater Sci Mater Med,* 2004, **15**, 493-496.
78. O. Harush-Frenkel, E. Rozentur, S. Benita and Y. Altschuler, *Biomacromolecules*, 2008, **9**, 435-443.
79. O. Harush-Frenkel, N. Debotton, S. Benita and Y. Altschuler, *Biochem Biophys Res Commun*, 2007, **353**, 26-32.
80. C. Wilhelm and F. Gazeau, *Biomaterials*, 2008, 29, 3161-3174.
81. X. Shi, T. P. Thomas, L. A. Myc, A. Kotlyar and J. R. Baker, *Phys Chem Chem Phys*, 2007, 9, 5712-5720.
82. V. Hirsch, C. Kinnear, M. Moniatte, B. Rothen-Rutishauser, M. J. Clift and A. Fink, *Nanoscale*, 2013, **5**, 3723-3732.

View Article Online
DOI: 10.1039/C3NR02861E

Graphical abstract

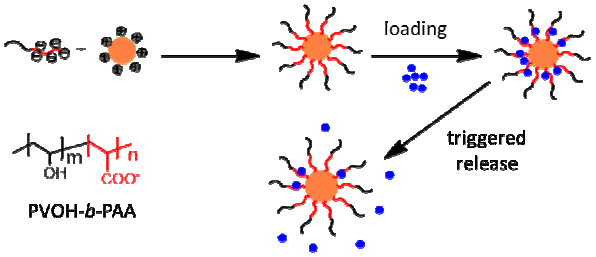

Original core/corona maghemite/poly(acrylic acid)-*block*-poly(vinyl alcohol) nanoparticles were evaluated as drug delivery systems sensitive to pH, ionic strength and/or temperature variations.